Environmental Science & Technology

Article

pubs.acs.org/est

Effect of Dissolved CO_2 on a Shallow Groundwater System: A Controlled Release Field Experiment

Robert C. Trautz,[†,*] John D. Pugh,[‡] Charuleka Varadharajan,[§] Liange Zheng,[§] Marco Bianchi,[§] Peter S. Nico,[§] Nicolas F. Spycher,[§] Dennis L. Newell,[∥] Richard A. Esposito,[‡] Yuxin Wu,[§] Baptiste Dafflon,[§] Susan S. Hubbard,[§] and Jens T. Birkholzer[§]

[†]Electric Power Research Institute, 3420 Hillview Avenue, Palo Alto, California 94304, United States

[‡]Southern Company Services, 600 North 18th Street, Birmingham, Alabama 35291, United States

[§]Lawrence Berkeley National Laboratory, Earth Science Division, 1 Cyclotron Road, Berkeley California 94720, United States

[∥]Los Alamos National Laboratory, Earth and Environmental Science Division (EES-14), Los Alamos, New Mexico 87545, United States

Supporting Information

ABSTRACT: Capturing carbon dioxide (CO_2) emissions from industrial sources and injecting the emissions deep underground in geologic formations is one method being considered to control CO_2 concentrations in the atmosphere. Sequestering CO_2 underground has its own set of environmental risks, including the potential migration of CO_2 out of the storage reservoir and resulting acidification and release of trace constituents in shallow groundwater. A field study involving the controlled release of groundwater containing dissolved CO_2 was initiated to investigate potential groundwater impacts. Dissolution of CO_2 in the groundwater resulted in a sustained and easily detected decrease of ~3 pH units. Several trace constituents, including As and Pb, remained below their respective detections limits and/or at background levels. Other constituents (Ba, Ca, Cr, Sr, Mg, Mn, and Fe) displayed a pulse response, consisting of an initial increase in concentration followed by either a return to background levels or slightly greater than background. This suggests a fast-release mechanism (desorption, exchange, and/or fast dissolution of small finite amounts of metals) concomitant in some cases with a slower release potentially involving different solid phases or mechanisms. Inorganic constituents regulated by the U.S. Environmental Protection Agency remained below their respective maximum contaminant levels throughout the experiment.

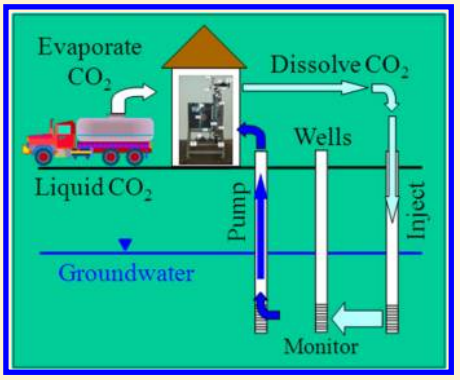

INTRODUCTION

Injecting CO_2 emissions deep underground in depleted oil and natural gas reservoirs, or rock formations containing brine too salty to drink, increases fluid pressure gradients, which can potentially push brine and CO_2 out of a storage reservoir through leakage pathways if they exist. Migration of brine into potable groundwater has the potential to degrade groundwater quality, because brines contain high concentrations of heavy metals, NaCl, and other major ions. Brine contamination associated with oil and natural gas operations is well documented in the literature.[1]

In contrast, CO_2 is less dense than water. Thus, in the absence of a pressure gradient, it can still leak from a storage reservoir into shallower zones by buoyancy forces alone. Geochemical alteration of shallow groundwater due to the presence of CO_2 is the focus of our study. CO_2 dissolution in groundwater causes increased acidity, which can potentially mobilize trace metals and ions by dissolving minerals containing these constituents found in natural sediments or by desorption/adsorption occurring at groundwater-sediment interfaces.[2−6] Concurrent precipitation of new mineral phases may also occur, resulting in the scavenging or depletion of some trace metals in groundwater.[7]

To date, experimental investigation of trace-element mobilization in response to CO_2 intrusion has mostly involved laboratory studies conducted on small samples of aquifer materials exposed to water and CO_2.[3,4] It is quite difficult, however, to replicate in situ field conditions in the laboratory: Changes in redox conditions in the field during sample collection can significantly alter subsequent laboratory results; natural variations in sediment mineralogy can lead to laboratory results that are not fully representative of much larger, geochemically heterogeneous sediment systems; overly aggressive batch experiments can produce results that are not truly representative of laminar groundwater flow; and differ-

Special Issue: Carbon Sequestration

Received: March 31, 2012
Revised: August 30, 2012
Accepted: September 5, 2012
Published: September 5, 2012

ences between field and laboratory scale can affect transport behavior and study conclusions. Therefore, field experiments are necessary to further assess the hydrogeochemical processes occurring in potable groundwater exposed to CO_2.[5]

The present paper provides an overview of an integrated field experiment, which consists of the controlled release of dissolved CO_2 into dilute groundwater in an isolated sand aquifer. The goals of the study were to investigate the potential impact that dissolved CO_2 has on in situ groundwater quality, to apply and test monitoring methods, and to evaluate geochemical modeling concepts and results. The test builds on previous experience gained in an earlier short-term field experiment performed in an unconfined groundwater system.[8,9]

Test Location, Site Characteristics, And Experimental Design. The field study was initiated in 2010, starting with hydrogeological characterization of the field site, field and laboratory characterization of groundwater and sediment, design and installation of a well field for injecting dissolved CO_2, design, and installation of the injection equipment, preinjection (background) groundwater monitoring, and an argon tracer test. Injection of dissolved CO_2 started on October 18, 2011 and ended 5 months later on March 23, 2012.

Site Setting. The controlled release field experiment is hosted by Southern Company Services (SCS) at the Victor J. Daniel Electric Generating Plant. Situated near the town of Escatawpa, Mississippi, Plant Daniel occupies approximately 650 ha of industrial and undeveloped land in a rural area of Jackson County, Mississippi. The Citronelle, Graham Ferry, and Pascagoula Formations, and the undifferentiated deposits of Miocene-age, are the primary sources of potable groundwater in Jackson County.[10] In general, the concentration of total dissolved solids (TDS) in groundwater increases with depth, eventually exceeding the U.S. Environmental Protection Agency (EPA) secondary drinking water criteria of 500 mg/L at a depth of about 425 m. The field site is shown in Figure 1. (Refer to Supporting Information for additional site background.)

Site Characterization. Site-characterization efforts were performed to identify and characterize a suitable groundwater system for dissolved CO_2 injection and to collect geochemical and hydrologic data needed for development of the reactive transport model discussed later in this paper.

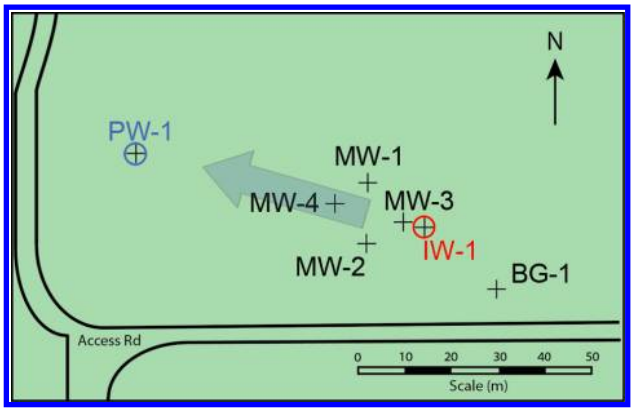

Figure 1. Site plan showing the pumping (PW-1), injection (IW-1), monitoring (MW-1 through MW-4), and background (BG-1) wells used during the controlled release experiment. The large arrow indicates the pumping/injection-induced groundwater flow direction. The distance between IW-1 and PW-1 is 63.4 m.

Hydrogeologic Field Characterization. An initial investigation was performed by installing three wells (IW-1, MW-1 and MW-2; Figure 1) and collecting geologic data to a depth of 56.7 m. The borings penetrated 30.5 m of sand and gravel of the Citronelle Formation, underlain by low-permeability clay from 30.5 to 46.9 m. Beneath the clay lies a gray-green fine-grained silty sand with minor clay, ranging from 46.9 to 54.6 m in depth, which served as the injection (i.e., test) interval. Believed to be in the uppermost section of the Graham Ferry Formation, the test sand is confined below by clay (Figure S1, Supporting Information). Cross-well seismic and complex resistivity tomograms were acquired between all monitoring wells, and gamma logs were collected in each well. Inversion and joint analysis of these baseline data suggests that the clay-rich unit that overlies the test interval is laterally continuous, and that the interval itself displays only minor heterogeneity. Geophysical monitoring of the dissolved CO_2 plume during injection is a major component of this study described further in a companion paper in this special issue.[11]

Multiple slug tests and a pumping well test were performed to measure the hydraulic properties of the test interval, which has an average horizontal hydraulic conductivity of 1.7×10^{-4} m/s and storativity of ~0.0003. Measured hydraulic conductivities exhibited a relatively narrow range (4.0×10^{-5}–1.8×10^{-4} m/s) suggesting the sand is rather homogeneous. The natural hydraulic gradient is very flat (0.0004 m/m), making it difficult to determine with accuracy the natural groundwater flow direction and velocity. Using the natural gradients, and assuming 30% porosity, the groundwater seepage velocities ranged from 0.01 to 0.02 m/d.

Laboratory Characterization of Sediments. Sediments collected during well installation, including sand from the test interval, clay from the upper confining layer, and thin "black laminations" found within the test interval, were characterized by a variety of laboratory- and synchrotron-based analysis. X-ray Diffraction (XRD) and thin-section petrographic analyses determined that the sand was dominated by large quartz grains with small fractions of albite, plagiclase, illite, and pyrite. The confining clay showed similar composition, with less quartz and a significant fraction of kaolinite. Total inorganic carbon (TIC) and total organic carbon (TOC) solid analyses were conducted using a Shimadzu TOC-VCSH high sensitivity inorganic–organic carbon analyzer with a SSM-5000A module. TIC and TOC measurements were below detection (~0.01%) for the sand, but showed 2.4% TOC for the black laminations.

Synchrotron-based X-ray absorption spectroscopy (XAS) and X-ray fluorescence (XRF) analyses were conducted at beamline 10.3.2 of the Advanced Light Source at Lawrence Berkeley National Laboratory (LBNL). The images in Figure 2 show the silicon (Si), iron (Fe), and sulfur (S) distribution within thin sections of the sand (A) and the black laminations (B). Linear combination fitting of iron X-ray absorption near-edge structure (XANES) spectra collected at the labeled points in the sand material confirmed that high Fe areas are dominated by illite (84% average of points 1–3) with smaller fractions of Fe (hydr)oxides (16% average of points 1–3). The areas with both Fe and S (seen as pink) are dominated by pyrite (86% point 4). The same was true for similar locations in the black laminated material (Figure 2B), with point 5 returning a fit of 86% pyrite and 14% FeS, and point 7 a composition of 94% illite with 6% Fe(II) as Fe(SO4). The large oblong feature in the upper center of Figure 2B (point 6) was seen as black in the thin section and shown to be rich in reduced sulfur groups, with

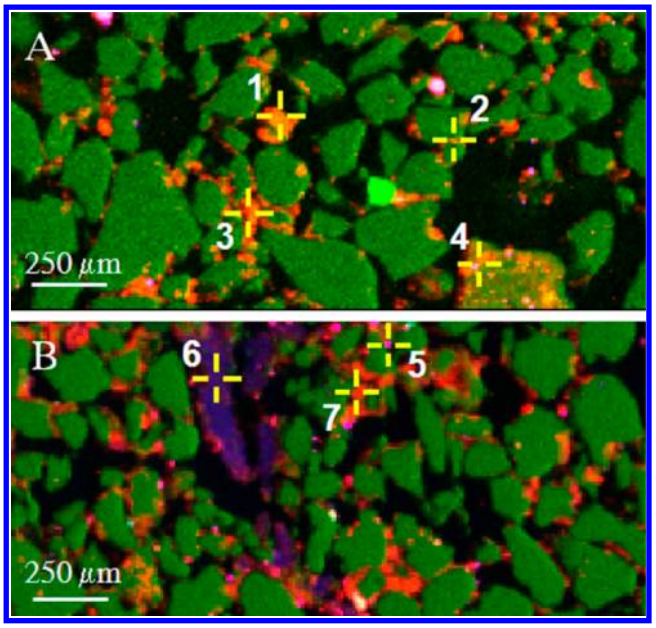

Figure 2. XRF maps showing the elemental distribution of Si (green), Fe (red), and S (blue) in (A) sand interval and B) black laminated material. XAS spectra were taken at the numbered locations (points 1−7) to confirm mineral form.

peaks in the sulfur XANES spectra at 2474.1 electron volts (eV) similar to those previously reported for thiols.[12] This is consistent with this material being rich in organic matter containing thiol functional groups. The sulfur XANES from point 5 confirmed its designation as pyrite, with sulfur XANES peaks at 2472.6 eV.[12] XRF spectra showed significant concentrations of As in some of the pyrite grains and some Pb. In the Fe-rich locations, the major spatial associated metals were Ca and Sr. Organic-rich features (point 6) also showed significant quantities of Ca, Sr, and Ge.

Table 1 shows the results of selective extractions performed on the sand and black laminations, including the material targeted by the extraction and the method used.[13−15] For all cases, there were significantly greater concentrations of metals extracted from the black laminations than from the sand. Significant quantities of Ca, Mg, and Sr were extracted under mild acetic acid conditions (pH = 5, extraction 1), indicating that these cations were either bound in trace carbonates or on easily exchangeable sites. Both the black laminations and sand material show release of Fe as a result of persulfate oxidation (extraction 4), confirming the presence of pyrite as indicated by the XRD and XAS.

Taken together, the above laboratory characterizations show that the test material is a quartz sand coated and interspersed with small amounts of Fe containing phyllosilicate clays, Fe (hydr)oxides, amorphous FeS, and pyrite. The presence of the organic-rich black laminations and the FeS and pyrite indicate a generally reducing environment. Selective extractions show that under the mild acidic conditions expected due to the CO_2 injection, significant quantities of divalent cations (e.g., Ca, Mg, Sr, and Mn) will likely be released either via cation exchange, dissolution of trace carbonates or other surface complexes. The release of metals and metalloids of concern is likely if dissolution of FeS or pyrite occurs, since these grains were identified as containing As and some fraction of Pb. Finally, on a mass basis, the black laminations may have a disproportionate impact on metal release due to elevated concentrations of both exchangeable cations and pyrite.

Buffering capacity of the sand material and the black laminations was determined by titration with 0.01 M HCl. A generic geochemical batch model was used to reproduce the titration curve. The pH buffering of the sediments was attributed primarily to protonation reactions. Carbonates were not detected in the sediments, and very small amounts potentially present (below analytical limits) were shown to have a negligible pH buffering effect compared to protonation (Figure S3). A reasonable fit to the data was obtained using the two reactions shown below with associated log(K) values (Figure S3). Reactions 1 and 2 are not tied with any particular mineral. It is assumed that the sediment as a whole (with volume fraction of one) is represented with one generic surface "SedOH", with a surface area of 10 m^2/g and a site density of 1 × 10^{-6} mol/m^2. Although these values, together with the fitted log(K) values, do not represent a unique set of parameter values, using these values in simulations (see Model Results section) ensures the same "generic" pH buffering behavior as in the titration experiment.

$$\mathrm{SedOH_2^+} = \mathrm{SedOH} + \mathrm{H^+}\ \log(K) = 0.5 \quad (1)$$

$$\mathrm{SedO^-} + \mathrm{H^+} = \mathrm{SedOH}\ \log(K) = 5.1 \quad (2)$$

The black laminations showed a greater buffering capacity, likely because of their higher organic-matter content; however, because of the unknown distribution of this material, its properties were not included in the model simulations.

Argon Tracer Test. A short-term tracer test using argon as a conservative species was conducted prior to the start of dissolved CO_2 injection to (1) provide confidence in the groundwater seepage velocities estimated from pumping tests (average velocity between the injection and pumping well is ∼0.08 m/d and ∼0.17 m/d using the hydraulic gradient at

Table 1. Selective Extraction Results for the Sand and Black Laminations from the Test Interval[a]

		sand material from test interval (μg/g)[b]					black laminations material from test interval (μg/g)[c]				
	extraction target [method]	Ca	Mg	Sr	Mn	Fe	Ca	Mg	Sr	Mn	Fe
1	carbonate bound [NaAcetate/acetic acid, pH = 5]	96 (14)	48 (7)	3.9 (0.5)	2.3 (0.2)	5 (6)	867	275	28	36	21
2	crystalline Fe (hydr)oxides [hydroxyl amine/acetic acid, 25% (v/v)]	130 (47)	73 (36)	4.8 (0.5)	3.5 (0.4)	119 (62)	820	265	24	30	755
3	amorphous FeS [6 N HCl]	84 (16)	46 (19)	3.1 (0.5)	2.8 (0.6)	98 (46)	749	210	16	29	232
4	pyrite [0.17 M $K_2S_2O_8$ in 0.2% (v/v) H_2SO_4]	98 (20)	41 (14)	3.6 (0.7)	1.3 (1.3)	216 (129)	755	212	16	8	816

[a]Significantly greater concentrations of trace metals were extracted from the black laminations compared to the sand material. [b]Average values from three measurements with standard deviations shown in parenthetical. [c]Values represent a single measurement (limited by available material).

MW-3) and used in the modeling effort; (2) to help assess the extent of hydrodynamic dispersion; and (3) to help in establishing an optimal sampling frequency during dissolved CO_2 injection.

Using the dipole pumping and injection scheme described in the next section, argon-saturated groundwater was injected into well IW-1 for a period of three days, and groundwater sampling to capture the argon pulse was focused at the nearest monitoring well (MW-3). (See Supporting Information S3.0 for argon sampling and analytical details.) Approximately 10 days after injection was initiated, argon concentrations began to rise above baseline, with a maximum value of ~7 ppm detected at 14 days (Figure 3). Argon concentrations returned to

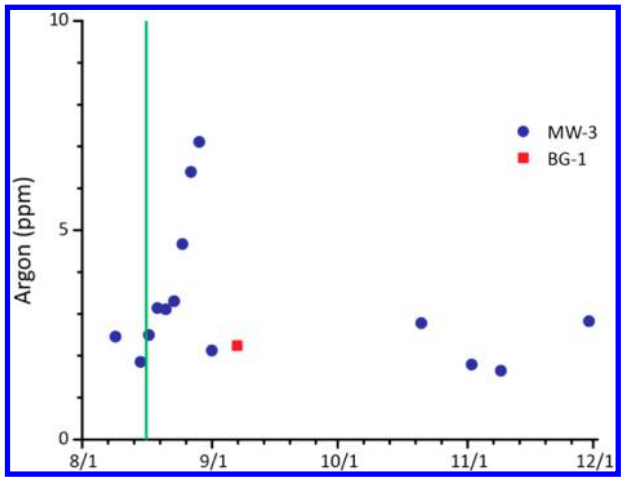

Figure 3. Dissolved argon concentration in groundwater collected at MW-3 during the argon tracer test. Green line marks the beginning of the Ar tracer test.

baseline conditions with certainty by mid-October, approximately 60 days after injection ended. Although the observed argon peak at MW-3 was not fully resolved, the observed breakthrough was consistent with seepage velocities (within 15%) previously estimated from pumping test analyses and was best matched with a limited dispersion (~0.1 m).

Measured argon concentrations in the injected groundwater ranged from 14 to 100 ppm (Table S1), which did not match the expected groundwater concentration (200 ppm) in the injected pulse based on argon solubility in water. The variability in the observed concentrations and underestimated target value may have resulted from incomplete argon saturation of the groundwater, leaking sample tubes or degassing within the samplers due to insufficient back pressure. Prior to the arrival of the argon pulse at MW-3, baseline argon concentrations in groundwater ranged from 2 to 3 ppm (Figure 3; Table S1). These values exceed the typical concentrations for air-saturated groundwater and groundwater with excess air,[16] likely reflecting analytical-detection limitations due to argon blank corrections with this method.

Fluid Delivery System. A hydrologic model was developed using the site characterization data to design the well field and optimize the flow rates needed to control the dissolved CO_2 plume during the experiment. The resulting well field (Figure 1) consisted of a dipole with groundwater being withdrawn from PW-1 and injected back into IW-1. The direction and extent of the injected dissolved CO_2 plume could then be controlled by adjusting the groundwater withdrawal and injection rates.

Groundwater was pumped from PW-1 at a constant rate (0.34 ± 0.04 L per second (L/s)) from the test interval to the land surface, where approximately two-thirds of the water was discharged to a surface water drain. The remaining one-third was infused with food-grade CO_2 (or argon) using a carbonation unit (held at or near subsurface pressures, 3.5−4 bar) before injecting it back into the sand at an average rate of 0.095 L/s (IW-1). Applying a groundwater pumping rate three times greater than the reinjection rate helped hydraulically control the distribution of carbonated groundwater by pulling it toward the pumping well, across intervening monitoring wells (MW-1 through MW-4), where groundwater quality samples were collected to measure impacts. The carbonation unit consisted of a contact membrane that saturated the groundwater with CO_2. Sealed piping was used to transport groundwater throughout the fluid delivery system, preventing it from coming in contact with air. This innovative design minimized oxidation of the groundwater, thus preserving in situ redox conditions that control biological activity, hydrogeochemical reactions in the subsurface, and the distribution of naturally occurring trace metals and ions dissolved in groundwater.

RESULTS AND DISCUSSION

Groundwater Trends in Response to CO_2 Injection. Groundwater quality samples were collected and analyzed for the constituents identified in Table S2 (Supporting Information). Samples were collected prior to dissolved CO_2 injection (baseline), during injection and after injection ended (post-injection). Baseline measurements were made under static (natural hydraulic gradient) and dynamic (forced hydraulic gradient) conditions prior to CO_2 injection to establish baseline trends. Static (i.e., prepumping) baseline monitoring started on September 2, 2010 and ended August 15, 2011, when groundwater pumping/injection began for the argon tracer test. (Note that pumping and injection continued for seven months nonstop through the end of CO_2 injection on March 23, 2012). The dynamic-baseline (pumping) period coincided with the first two months of pumping/injection prior to injecting dissolved CO_2 on October 18, 2011. Table S3 (Supporting Information) lists the number of background sampling events conducted for each well prior to (1) pumping and (2) the initiation of carbonated water injection. The various testing periods are shown on Figures 4 and 5.

Because of its proximity to the injection well, MW-3 was the first well to exhibit impacts resulting from CO_2 injection, and is the focus of this analysis. Figure 4 shows the evolution of pH, conductivity, and alkalinity in MW-3. A pronounced and sustained decrease in pH (to about 5.1) can be seen in response to the arrival of dissolved CO_2, starting 8−10 days after injection was initiated. Conductivity and alkalinity start to increase from their baseline values at about the same time. However, compared to the pH trend, conductivity and alkalinity exhibit a sharp and short-term pulse behavior, with peak values reached after about 23 to 24 days. The decrease in alkalinity concentration most likely reflects the increasing protonation of dissolved TIC from HCO_3^- to $H_2CO_3^0$ (pK about 6.3 at 25 °C) as pH continues to decline. The observed trend limits the practical use of field alkalinity and conductivity measurements as early indicators of dissolved CO_2 arrival, detection of which is highly dependent upon the sampling

dx.doi.org/10.1021/es301280t | Environ. Sci. Technol. 2013, 47, 298−305

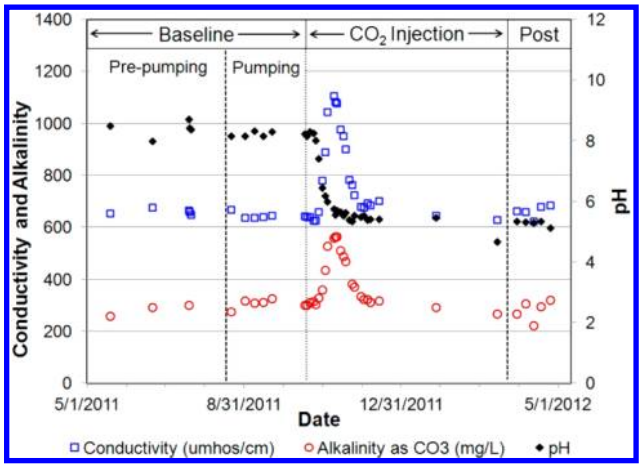

Figure 4. In situ pH, electrical conductivity and alkalinity measurements over time at MW-3 showing a sharp and short-term increase in conductivity and alkalinity (blue squares and red circles), and a sharp and sustained decrease in pH (black diamonds).

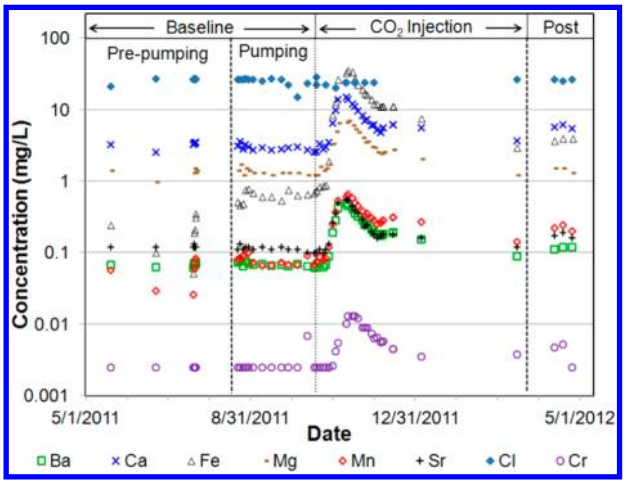

Figure 5. Major and minor cation concentrations over time at MW-3, showing short-term increases after initiation of CO_2 injection, followed by stabilizing but elevated concentrations over the long-term. Chloride concentrations are also shown (blue diamonds) and did not respond to CO_2 injection, which is typical of the anions.

frequency and aquifer properties. In contrast, the pH and total dissolved carbonate content (here calculated to reach ~130 mM, or about 5700 ppm as dissolved CO_2) would be excellent indicators. Overall, the transport behavior in response to dissolved CO_2 injection is similar to the transport behavior observed during the argon tracer test.

Figure 5 shows concentrations of selected major cations, minor cations and chloride over time. Concentrations measured in preinjection baseline groundwater samples showed minor variation (or were below detection limits). Molybdenum concentrations exhibit slight fluctuations (not shown) during pumping conditions, suggesting that this species could be sensitive to pumping/injection activities. With the exception of bicarbonate alkalinity included in Figure 4, anion concentrations exhibited no significant trends (see chloride in Figure 5).

Modeling Results. A reactive transport model was developed to facilitate the design of the test, guide test operations, and interpret observed concentrations of dissolved species. Modeling was conducted with the multiphase and multicomponent reactive transport simulator TOUGHREACT, version 2.[17]

The sandy test interval was represented using a horizontal two-dimensional depth-averaged model domain of about 500 by 500 m lateral extent and 6 m thick. An area of 20 by 40 m surrounding the injection and monitoring wells was finely discretized into a honeycomb mesh, with gridblock sizes around 0.5 m (Figure S4). Hydraulic properties of the aquifer and geochemical analyses of sediments described earlier were used as input to the model. Hydrodynamic dispersion was not specifically computed and approximated with numerical dispersion (approximately corresponding to dispersivity values ~0.25 m). The numerical dispersion is of the same order of magnitude as the hydrodynamic dispersion derived from the Ar tracer test. The seepage velocity was determined from the pumping test analyzes and porosity estimates, and later confirmed by analyzing the Ar data using a finely discretized MT3DMS model that included dispersion (best fit ~0.1 m). The modeled flow field is shown in Figure S5.

The chemical compositions of initial and injected waters used in the simulations (Table S4) reflected average concentrations of 74 baseline groundwater samples. Under baseline conditions, the groundwater composition remained essentially constant, with pH in the range between 7.4 and 8.6. As a result, the saturation indices for minerals and redox potentials computed for individual water analyses did not differ significantly from those computed using average concentrations, with average pH 7.9 and a reasonable charge-balanced average composition. Redox disequilibrium was suggested by these data and taken into account by controlling redox for chemical phases other than ferrous and ferric phases with HS^-/SO_4^{-2} (initial E_h about −0.29 V), and for ferrous and ferric phases with Fe^{2+}/Fe^{3+} (initial Eh about 0.16 V). The composition of the injected water was obtained by equilibrating the initial water with a P_{CO2} of 3.8 bar, which yields a pH of ~5.

As observed in the sediment mineralogical analyses, iron minerals in the target formation consisted mainly of Fe-bearing clays and silicates, with some iron (hydr)oxides and trace iron sulfides. Correspondingly, the geochemical model considered illite, Fe-smectite, ferrihydrite (as $Fe(OH)_3(s)$) and amorphous iron sulfide (mackinawite, FeS(m)), in addition to major aquifer minerals such as quartz and K-feldspar. The amount of FeS(m) was estimated from the selective extraction data (~0.02 vol%), and the amount of $Fe(OH)_3(s)$ from the sediment acid titration data (~0.04 vol%, assuming this phase dominates H^+ sorption, as a first approximation), described earlier in the paper. Carbonates were not detected using XRD and solid TIC-TOC analysis. However, geochemical speciation analyses, selective extractions and correlations between aqueous Ca, Mg and bicarbonate concentrations before and after injection lead us to postulate that small amounts of dolomite could be present in the sandy test interval. Therefore, trace amounts of dolomite were included in the simulations (0.006 vol%, below the XRD and TIC-TOC analyzer detection limits). The amount of illite, smectite, quartz, and K-feldspar were roughly estimated from examinations of sediment cores and thin sections.

The reactive transport model considers aqueous complexation, mineral dissolution, and precipitation under kinetic constraints (e.g., ref 18), cation exchange (for Ca, Mg, K, Na, Ba, Mn and Sr, using data from ref 19), and surface complexation (for H^+, HCO_3^-, and Cr, using data from refs

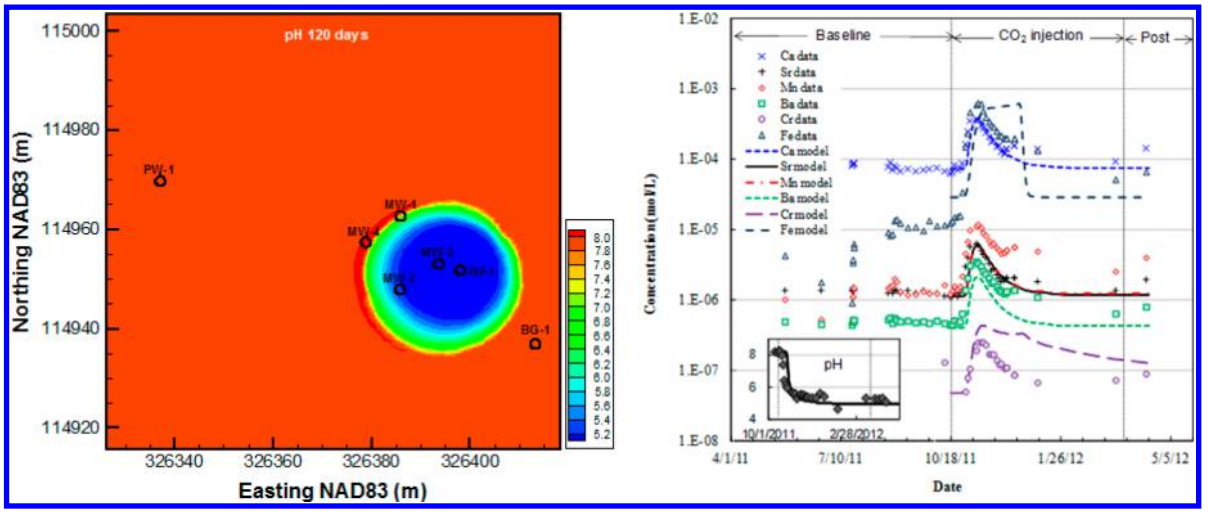

Figure 6. Predicted pH plume at 120 days after injection started (pretest simulation) and predicted (lines) breakthrough of pH, Ca, Sr, Mn, Ba, Cr, and Fe at well MW-3 compared to observations (symbols).

20 and 21). Other thermodynamic data were taken primarily from the eq 3/6 V8.1 geochemical modeling package.[22,23]

The reactive transport model was used to assess the groundwater-quality response to carbonated water injection. Pretest predictions of pH (dropping to ~5.5) were very much in line with test observations (Figure 6), with low-pH breakthrough occurring first at MW-3 then, in order of arrival, at MW-2, MW-1, and MW-4. A conceptual model developed by Zheng[9] to explain the release of metals at another CO_2 injection field test site was tested. In this conceptual model, it is postulated that the drop in pH induces the dissolution of carbonates (here assumed to be dolomite). The resulting increase in Ca and Mg concentrations subsequently triggers a series of cation exchange reactions, which result in an increase in the concentrations of alkaline earth cations and Mn. Slight increases in Cr (occurring mostly as an oxyanion) were attributed to desorption, and the dissolution of Fe sulfide was assumed to contribute to the observed significant increase in Fe concentrations. The simulations reproduce closely the measured breakthrough at MW-3 for pH, bicarbonate, Ca, Mg, K, Sr, and to a lesser extent, the trends of Mn, Ba, Cr and Fe (Figure 6).

The model underestimates the Mn and Ba concentrations. This might be attributed to the uncertainty of parameters adopted in the model, such as ion selectivities and cation exchange capacities, or presence of impurities in carbonate or other minerals (not included in the model) and released during dissolution of these phases. The model cannot reproduce the observed sharp Cr and Fe peaks but predicts concentrations in the range of observed values. This could be the consequence of excessive initial Cr loading in the model, which depends on input specific surface area and site density values with large uncertainties. For iron, the release is modeled by the dissolution of Fe minerals. It is possible that other processes such as desorption, or dissolution of other Fe-bearing minerals, or different input parameters affecting dissolution rates might have to be considered. It should be noted that no parameter calibration was conducted, which could be used to improve the model fit to the observed data.

The concentrations of other trace metals appeared either unaffected by the test or remained below detection limits. Note that the observed and predicted pulse behavior of released metals implies that a quick depletion of these metals (from the sediments) must take place at the front of the plume, such that the trailing part of the plume encounters a source that has been depleted by continuous mobilization at the plume front. In our case, small finite amounts of fast-dissolving carbonates are assumed to be the source of Ca and Mg, although it should be noted that finite amounts of Ca and Mg desorbing from organics or hydroxides would yield a similar pulse behavior. This possibility, as well as desorption of Fe(II) from Fe(III) hydroxides[21] or other cases of metal-mineral associations are being further investigated, including comparative modeling studies using different numerical models.

DISCUSSION

A controlled release field experiment is presented that uses an integrated approach to study geochemical processes affecting CO_2-induced mobilization of trace metals and major ions in groundwater. Preinjection field and laboratory site characterization data were used to develop a conceptual model of the site and parametrize a groundwater flow and transport model used to design and simulate the field experiment. Once implemented, the design proved to be an effective method of controlling the release of dissolved CO_2, and ensuring that changes in groundwater quality were caused primarily by CO_2 and not external factors (e.g., cross-contamination by air). The negligible difference between the static (prepumping) and dynamic (pumping) baseline concentration data (Figures 4 and 5), reinforces this claim, indicating that the forced hydraulic gradient caused by pumping/injecting groundwater had little influence on groundwater quality prior to CO_2 injection.

Mobilization of major and minor cations in response to CO_2 injection is evident from the short-term concentration increases coinciding with the arrival of dissolved CO_2, but these increases are followed by stabilizing yet slightly elevated concentrations over the longer term (Figure 5). On the basis of an intrawell comparison for MW-3, statistically significant increases above baseline concentrations have been observed for Ba, Be, and Cr during multiple sampling events, and for Hg and Sb during one sampling event. Inorganic constituents regulated by the EPA have remained below their respective maximum contaminant levels (MCLs). Of all regulated constituents exhibiting

Table 2. Minimum and Maximum Concentrations Observed during the Baseline, CO_2-Injection and Post-Injection Monitoring Periods for MW-3, Statistical Significance, and Comparison to EPA Primary Drinking Water Standards[a]

		static and dynamic baseline		co_2 injection and post-injection					
parameter	unit	min.	max.	min.	max.	MDL	EPA MCL	significant?	above MCL?
arsenic	mg/L	<0.0013	<0.0013	<0.0013	<0.0013	0.0013	0.01	no	no
barium	mg/L	0.055	0.11	0.062	0.48	0.0013	2	yes	no
beryllium	mg/L	<0.00025	<0.00025	<0.00025	0.00072	0.00025	0.004	yes	no
chromium	mg/L	<0.0025	0.007	<0.0025	0.013	0.0025	0.1	yes	no
copper	mg/L	<0.0011	0.002	<0.0011	0.001	0.0011	1.3	no	no
fluoride	mg/L	0.18	0.58	0.051	0.43	0.0035	4	no	no
mercury	mg/L	<0.00007	0.00017	<0.00007	0.00023	0.00007	0.002	yes	no
lead	mg/L	<0.0002	0.0009	<0.0002	<0.0002	0.0002	0.015	no	no
antimony	mg/L	<0.0023	<0.0023	<0.0023	0.003	0.0023	0.006	yes	no
selenium	mg/L	<0.001	<0.001	<0.001	<0.001	0.001	0.05	no	no
thallium	mg/L	<0.0005	<0.0005	<0.0005	<0.0005	0.0005	0.002	no	no

[a]Statistical significance, MCL = maximum contaminant level, MDL = method detection limit.

statistically significant increases at MW-3, Sb was the closest to exceeding its MCL at one-half the regulated limit (Table 2).

The dissolution of CO_2 in the groundwater resulted in a sustained and easily detected drop of ~3 pH units. However, many trace constituents, including As and Pb, remained below their respective detections limits throughout the experiment, suggesting that they either were not present at significant solid concentrations, or were scavenged by competing precipitation processes. Observed and modeled time profiles for Ca, Sr, Mg, Ba, Mn, and Fe display a pulse response followed by either a return to background conditions or to concentrations slightly greater than background. This suggests a fast release mechanism with depletion of metals from their source at the front of the low-pH plume (such as desorption, exchange, or fast dissolution of small finite amounts of minerals), possibly overlapping with a slower and more continuous release from mineral dissolution. While the modeling analyses presented here support one plausible explanation for observed concentration trends, further work is needed to narrow down possible mechanisms at play and improve our fundamental understanding of geochemical processes that lead to CO_2-induced mobilization of trace metals in groundwater.

The data obtained in this study are extremely valuable for calibrating and validating computer models used to predict the fate and transport of CO_2, as well as determining the potential for mobilization of trace metals and the effectiveness of various monitoring/characterization techniques. A full understanding of metal-sediment associations and biogeochemical mechanisms contributing to metal release and uptake in the subsurface, together with accurate-as-possible numerical model predictions, are key to evaluating the environmental risks associated with CO_2 storage and the long-term performance of individual storage facilities. The development of such conceptual and numerical models are essential to formulating future strategies for remediating CO_2 impacted groundwater (should it be needed), and to informing stakeholders (including the public, regulators, and industry) of the efficacy and risks associated with individual projects.

■ ASSOCIATED CONTENT

Supporting Information

Additional S1.0 site background information; S2.0 argon tracer sampling and analysis procedures; S3.0 list of constituents routinely analyzed during the study; S4.0 groundwater monitoring frequency; and S5.0 model details including mesh configuration and initial groundwater conditions. This information is available free of charge via the Internet at http://pubs.acs.org/.

■ AUTHOR INFORMATION

Corresponding Author

*Phone: 650-855-2088. Fax 650-855-2511. E-mail: rtrautz@epri.com.

Notes

The authors declare no competing financial interest.

■ ACKNOWLEDGMENTS

This work was supported by the Electric Power Research Institute; the EPA, Office of Water, under an Interagency Agreement with the U.S. Department of Energy (DOE) at LBNL, under contract number DE-AC02-05CH11231; and the Assistant Secretary for Fossil Energy, National Energy Technology Laboratory (NETL), National Risk Assessment Program (NRAP), of the US Department of Energy under Contract No. DEAC02-05CH11231.

■ REFERENCES

(1) Gleason, R. A.; Thamke, J. N.; Smith, B. D.; Tangen, B. A.; Chesley-Preston, T.; Preston, T. M. *Examination of Brine Contamination Risk to Aquatic Resources from Petroleum Development in the Williston Basin*, U.S. Geological Survey Fact Sheet 2011-3047; United States Department of Interior: Washington, DC, 2011; 4 p.

(2) Zheng, L.; Apps, J. A.; Zhang, Y.; Xu, T.; Birkholzer, J. T. On mobilization of lead and arsenic in groundwater in response to CO_2 leakage from deep geological storage. *Chem. Geol.* **2009**, *268* (3−4), 281−297.

(3) Little, M. G.; Jackson, R. B. Potential impacts of leakage from deep CO_2 geosequestration on overlying freshwater aquifers. *Environ. Sci. Technol.* **2010**, *44* (23), 9225−9232.

(4) Lu, J. M.; Partin, J. W.; Hovorka, S. D.; Wong, C. Potential risks to freshwater resources as a result of leakage from CO_2 geological storage: A batch-reaction experiment. *Environ. Earth Sci.* **2010**, *60* (2), 335−348.

(5) Apps, J. A.; Zheng, L.; Zhang, Y.; Xu, T.; Birkholzer, J. T. Evaluation of groundwater quality changes in response to CO_2 leakage from deep geological storage. *Trans. Porous Media* **2010**, *82* (1), 215−246.

(6) Wilkin, R. T.; Digiulio, D. C. Geochemical impacts to groundwater from geologic carbon sequestration: Controls on pH and inorganic carbon concentrations from reaction path and kinetic modeling. *Environ. Sci. Technol.* **2010**, *44* (12), 4821−4827.

(7) Keating, E. H.; Fessenden, J.; Kanjorski, N.; Daniel, J.; Koning, D. J.; Pawar, R. The impact of CO_2 on shallow groundwater chemistry: Observations at a natural analog site and implications for carbon sequestration. *Environ. Earth Sci.* **2010**, *60* (3), 521−536.
(8) Kharaka, Y. K.; Thordsen, J. J.; Kakouros, E.; Ambats, G.; Herkelrath, W. N.; Beers, S. R.; Birkholzer, J. T.; Apps, J. A.; Spycher, N. F.; Zheng, L.; Trautz, R. C.; Rauch, H. W.; Gullickson, K. S. Changes in the chemistry of shallow groundwater related to the 2008 injection of CO_2 at the ZERT field site, Bozeman, Montana. *Environ. Earth Sci.* **2010**, *60* (2), 273−284.
(9) Zheng, L.; Apps, J. A.; Spycher, N.; Birkholzer, J. T.; Kharaka, Y. K.; Thordsen, J. J.; Beers, S. R.; Herkelrath, W. N.; Kakouros, E.; Trautz, R. C. Geochemical modeling of changes in shallow groundwater chemistry observed during the MSU-ZERT CO_2 injection experiment. *Int. J. Greenhouse Gas Control* **2011**, *7* (C), 202−217.
(10) Slack, L. J.; Oakley, W. T.; Cooper, L. M. *Quality of Groundwater in Jackson County, Mississippi, March−June 1993*; United States Department of Interior, U.S. Geological Survey Open-File Report 93−479, U.S. Government Printing Office: Washington, DC, 1993.
(11) Dafflon, B.; Wu, Y.; Hubbard, S. S.; Birkholzer, J.; Daley, T.; Pugh, J.; Peterson, J. E.; Trautz, R. Monitoring CO_2 intrusion and associated geochemical transformations in a shallow groundwater system using complex electrical method. *Environ. Sci. Technol.* **2012**, DOI: 10.1021/es301260e.
(12) Vairavamurthy, A. Using X-ray absorption to probe sulfur oxidation states in complex molecules. *Spectrochim. Acta, Part A* **1998**, *54* (12), 2009−2017.
(13) La Force, M. J.; Fendorf, S. Solid-phase iron characterization during common selective sequential extractions. *Soil Sci. Soc. Am. J.* **2000**, *64*, 1608−1615.
(14) Roth, D. A.; Taylor, H. E.; Domagalski, J.; Dileanis, P.; Peart, D. B.; Antweiler, R. C.; Alpers, C. N. Distribution of inorganic mercury in Sacramento River water and suspended colloidal sediment material. *Arch. Environ. Contam. Toxicol.* **2001**, *40*, 161−172.
(15) Cornwell, J. C.; Morse, J. W. The characterization of iron sulfide minerals in anoxic marine sediments. *Marine Chem.* **1987**, *22* (2−4), 193−206, DOI: 10.1016/0304-4203(87)90008-9.
(16) Heaton, T. H. E.; Vogel, J. C. "Excess Air" in Groundwater . *J. Hydrol.* **1981**, *50*, 201−216.
(17) Xu, T.; Spycher, N.; Sonnenthal, E.; Zhang, G.; Zheng, L; Pruess, K. TOUGHREACT Version 2.0: A simulator for subsurface reactive transport under non-isothermal multiphase flow conditions. *Comput. Geosci.* **2011**, *37* (6), 763−774.
(18) Steefel, C. I.; Lasaga, A. C. A coupled model for transport of multiple chemical species and kinetic precipitation/dissolution reactions with applications to reactive flow in single phase hydrothermal system. *Am. J. Sci.* **1994**, *294*, 529−592.
(19) Appelo, C. J. A.; Postma, D. *Geochemistry, Groundwater and Pollution*; A. A. Balkema: Rotterdam, the Netherlands, 1994.
(20) Dzombak, D. A.; Morel, F. M. M. *Surface Complexation Modeling-Hydrous Ferric Oxide*; John Wiley & Sons: New York, 1990.
(21) Appelo, C. A. J.; Van Der Weiden, M. J. J.; Tournassat, C.; Charlet, L. Surface complexation of ferrous iron and carbonate on ferrihydrite and the mobilization of arsenic. *Environ. Sci. Technol.* **2002**, *36* (14), 3096−3103.
(22) Wolery, T. J. *EQ3/6, A Software Package for Geochemical Modelling of Aqueous System*; UCRL-MA 110662, Lawrence Livermore National Laboratory: Livermore, CA, 1993.
(23) Johnson, J. W.; Oelkers, E. H.; Helgeson, H. C. SUPCRT92: A software package for calculating the standard molal thermodynamic properties of minerals, gases, aqueous species, and reactions from 1 to 5000 bar and 0 to 1000°C. *Comput. Geosci.* **1992**, *18* (7), 899−947.